Mechanisms of Grain Refinement in Aluminum Alloys during Severe Plastic Deformation

R.Kaibyshev, I.Mazurina

Institute for Metals Superplasticity Problems RAS, 450001, Khalturina 39, Ufa, Russia

Keywords: Recrystallization and Recovery, Aluminum Alloys, Intense Plastic Straining, Grain boundaries, Thermomechanical Processing

Abstract. The mechanisms of grain refinement during severe plastic deformation have been studied, by comparing the microstructure evolution in an AA2219 aluminium alloy, containing Al_3Zr nanoscale particles, with that in a dilute Al-3%Cu alloy deformed identically by equal-channel angular extrusion (ECAE) at 250°C to a maximum strain of ~12. Transmission electron microscopy (TEM) was used on the AA2219 alloy to reveal the misorientations of deformation-induced boundaries. Microstructural evolution in the Al-3%Cu alloy was studied by electron-back scattering diffraction (EBSD) orientation mapping. It was shown that the mechanism of grain refinement in the AA2219 alloy is continuous dynamic recrystallization (CDRX) consisting of two main elementary processes. In the initial stages of plastic deformation, the formation of three-dimensional arrays of low-angle boundaries (LABs) takes place. Further strain results in increasing misorientation of these boundaries providing their gradual transformation into high-angle boundaries (HABs). A fully recrystallized structure with an average grain size of ~0.9 μm is evolved after a total strain of ~12. In the dilute Al-Cu alloy the evolution of ultrafine grains with an average size of ~6 μm is attributed to the formation of deformation bands outlined by HABs and extended medium to high-angle boundaries at moderate strains. The subdivision of these deformation bands into fine grains rarely occurs through the mechanism of geometric recrystallization (GRX). In this alloy the main contribution in the grain refinement gives CDRX occurring within fibrous structural features. At ε~12, a partially recrystallized structure is formed in the Al-3%Cu alloy.

Introduction

There is significant commercial interest in the development of aluminum alloys with ultra-fine grain structure for structural applications due to the fact that extensive grain refinement has many technological benefits and may increase the strength and toughness of materials at room temperature. [1]. The most attractive method for achieving submicron-scale grain size in aluminum alloys is the application of very large plastic strains through techniques in which a sample can be deformed without any net change in its dimensions [2]. The most popular technique for subjecting a bulk material to intense plastic straining (IPS) at the laboratory scale is equal-channel angular extrusion (ECAE) [2]. Recently, several reports dealt with the characterization of the microstructures and mechanical properties of aluminum alloys processed by ECAE [3]. However, the mechanisms leading to grain refinement in pure Al and aluminium alloys under ECAE processing have only been the object of a limited number of studies [4-10]. In addition, very few systematic studies have employed orientation imaging microscopy (OIM) to examine the evolution of misorientation distribution with strain [4,8-10]. As a result, the exact structural mechanisms responsible for the formation of ultra-fine grains in aluminium alloys during ECAE are still unknown. There exist two main concepts of the structural changes taking place during severe plastic deformation in aluminium alloys.

Authors [2,8] suggested that at low temperatures, the grain refinement to the submicron level in aluminium alloys under ECAE occurs by the extension and compression of grain boundaries with strain followed by subdivision of ribbon grain structure by transverse high-angle boundaries (HAB) being formed discontinuously. It was assumed that this process provides the major fraction of

resulting HABs. The formation of additional deformation-induced boundaries as geometrically necessary dislocation boundaries (GNB) [8] plays a minor role in the grain refinement. This mechanism is based on the assumption that the original grains are deformed as the whole sample due to a limited number of active dislocation slip systems. It is worth noting that this mechanism was suggested on the base of OIM observations of microstructure evolution in dilute aluminium alloys and aluminum alloys containing micron-scale second-phase particles.

The other mechanism of grain refinement, continuous dynamic recrystallization (CDRX), was suggested in work [11] in which the microstructural evolution of an Al-Mn alloy containing submicron-scale second-phase particles was examined after ECAE. Recently, Belyakov et al. [12,13] showed that in materials with fcc lattice such as copper and austenitic steel new nanoscale grains could result from a kind of continuous reaction, i.e. CDRX. It is known [14,15] that the process of CDRX resulting in micron-scale grains involves two main elementary mechanisms:

(i) the formation of arrays of low-angle subboundaries;

(ii) the transformation of low-angle boundaries (LABs) into true high-angle boundaries (HABs) due to a gradual increase in misorientation of LABs with strain.

It was shown that CDRX results in submicron-scale grains in aluminum alloys contaning a high volume fraction of nanoscale dispersoids [16-18].

The aim of the present work is to report the mechanisms of grain refinement in a dilute Al-3%Cu alloy and an Al-6%Cu alloy containing dispersoids during severe plastic deformation at a similar temperature of 250°C. Microstructural evolution in the both materials was studied by the OIM technique.

Materials and experimental procedures

The 2219 aluminum alloy with a chemical composition of Al-6.4%Cu-0.3%Mn-0.18%Cr-0.19%Zr-0.06%Fe (in weight pct), denoted as AA2219 herein, and the Al-3%Cu alloy were manufactured by direct chill casting. The AA2219 and Al-3%Cu alloys were subjected to solution treatment at 530°C for 6 hours and 520°C for 4 hours, respectively. Next, both ingots were finally cut into cylinders with 20 mm diameter and 100 mm length. The initial grain size was ~140 μm in the AA2219 alloy. Initial structure in the Al-3%Cu was non-uniform with different areas in the material possessing average grain sizes of ~120 μm and ~450 μm.

The ECAE pressing was carried out in air using an isothermal die with a circular internal cross-section. The channel had an L-shaped configuration. Deformation through this die produces a strain of ~1 on each passage [6]. Repetitive extrusion up to fixed pressings was used to achieve high strains. Route A in which the specimen is removed from the die and the pressing is repeated without any rotation of the sample [4,6,11] was used. The repetitive extrusion was continuously conducted without any intermediate holdings in a furnace. Total time, at which the specimen was held at deformation temperature during ECAE processing, was ~15 min per each extrusion pass. The specimens were water quenched after ECAE pressings to the strains of ~1, ~2, ~4, ~8 and ~12.

Following ECAE, each sample was sectioned parallel to the extrusion directions, and the deformed structure was characterized at the centre of the die symmetry plane [8]. Discs of 3mm diameter were cut from these slices and then ground to a thickness of ~0.25 mm. Misorientation analysis of the Al-3%Cu was carried out by the EBSD technique. For this purpose, these discs were lightly electropolished to give a strain-free surface. EBSD orientation maps were acquired using a LEO-1530 SEM fitted with automated HKL-EBSD pattern collection system with a spatial resolution of ~500 nm and an angular resolution of ~0.5° provided by Oxford Instruments. Arbitrary areas were automatically scanned with 1 μm steps. HABs were defined as being greater than, or equal to, 15° in misorientation and low-angle boundaries (LAB) as having a misorientation less than 15°. HABs and LABs are depicted in OIM maps as dark and light lines, respectively.

Misorientation analysis of the AA2219 alloy was performed by the TEM technique. For TEM analysis similar discs were electropolished to perforation with a Tenupol-3 twinjet polishing unit using a standard $75\%CH_3COOH+25\%HNO_3$ solution at -30°C and 20V. The thin foils were examined using a Jeol-2000EX TEM with a double-tilt stage at an accelerating potential of 160 kV. All the clearly defined (sub)grain boundaries were taken into account to determinate the (sub)boundary misorientations. Misorientations of the deformation-induced boundaries were analysed using the conventional Kikuchi-line technique [19]. The accuracy of the measurements was about 0.8°. The (sub)boundary misorientations were determined from, at least, four arbitrary selected typical areas for each specimen. A total of ~60 (sub)boundaries were analysed for each sample.

Experimental results

The AA2219 alloy. Apparently, the structures evolved in the AA2219 alloy are essentially homogeneous. At $\varepsilon \leq 2$, two types of subgrains were formed. Elongated subgrains alternate with areas of essentially equiaxed subgrains. At $\varepsilon \sim 2$, isolated segments of deformation-induced boundaries acquire increased misorientation, which is significantly higher than the misorientation of the whole boundary. Deformation-induced boundaries have low-angle origin (Fig.1a). It is seen that three-dimensional arrays of LABs were evolved.

At $\varepsilon \sim 4$, the formation of deformation-induced HABs was detected in the vicinity of some initial boundaries (Fig.1b). Mixed arrays of LABs and HABs were found at this strain. In general, the deformed structure consists of elongated crystallites comprising band-like features (Fig. 2a) that are approximately aligned in the shear direction. Most of these longitudinal boundaries have high-angle origin, whereas the transverse boundaries have low-angle or moderate-angle misorientation. The average misorientation of the transverse boundaries is $\sim 11^{\circ}$ (Fig. 2b). Notably the deformation-induced LABs are predominant within the initial grain interiors; near old boundaries the deformation-induced boundaries have high-angle origin.

Upon further strain the average misorientation of deformation-induced boundaries becomes higher than 15° (Figs. 1c and 2b). Three-dimensional arrays of HABs are formed (Fig. 1c). At $\varepsilon \sim 8$, true recrystallized grains outlined by HABs from all sides were revealed (Fig. 2b). However, crystallites surrounded by both HABs and LABs dominate. Notably, the continuous boundaries aligned in the shear direction consist of isolated segments having high-angle misorientation alternating with segments with low-angle misorientation. It is seen that extensive formation of transverse LABs takes place within elongated (sub)grains (Fig. 1c) which acquire equiaxed shape (Figs. 1c and 2a). As a result, an average misorientation of transverse boundaries is less than that of longitudinal boundaries aligned in the shear direction (Fig. 2b). Further strain leads to an increasing fraction of recrystallized grains. The volume fraction of the true recrystallized grains surrounded by HABs from all sides (Fig. 3) at $\varepsilon \sim 12$ is about 85%. The misorientation of the longitudinal HABs increases with strain, whereas the average misorientation of the transverse boundaries remains essentially unchanged (Fig. 2b). The latter point is attributed to the persistent formation of transverse LABs within new grains elongated in the shear direction (Fig. 2a).

The parameters of deformed microstructure as a function of strain are summarized in Fig. 2a. It is seen that the (sub)grain size, d, tends to decrease with increasing strain. This decrease in the average grain size is attributed to the subdivision of the elongated (sub)grains by transverse LABs resulting in a decrease in the grain aspect ratio, defined as the ratio of the grain dimension in the shear direction to that in the transverse direction. This subdivision provides more a equiaxed shape of the average, new grains (Fig. 2a).

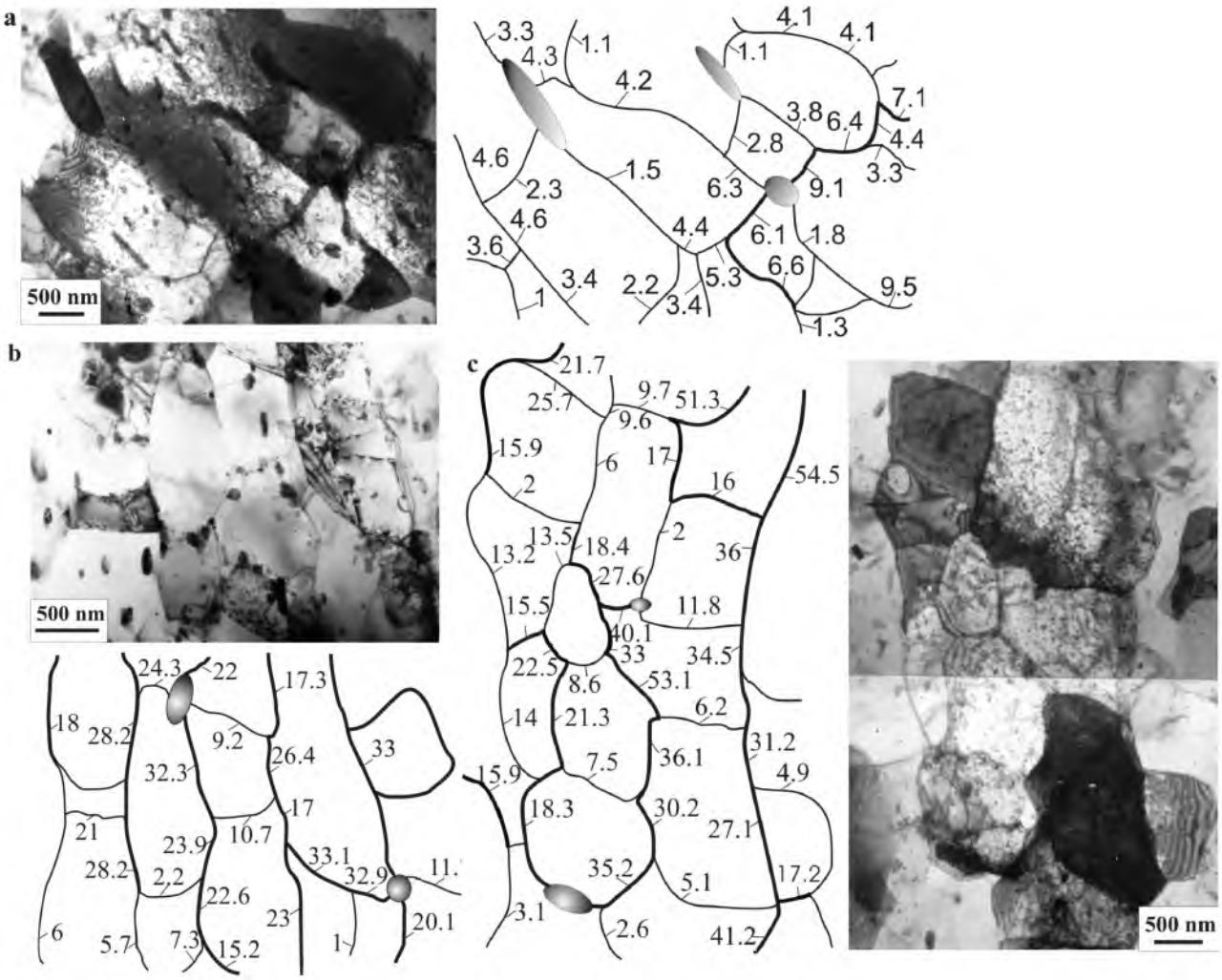

Fig. 1. The microstructures and associated misorientation maps of AA2219 deformed by ECAE at 250°C to: (a) ε=2, (b) ε=4; (c) ε=8

In particular, the size of the equiaxed crystallites and the distance between the transverse boundaries are essentially the same at ε≥4 (Fig. 2a). At ε≥8, the newly formed grains are elongated in the shear direction. Fig. 2b demonstrates the change in average misorientation angle θ_{ave} of the deformation-induced boundaries with strain. The average misorientation, θ_{ave}, between (sub)grains (Fig. 2b) and the population of HABs (Fig. 3) increases at ε>2. At lower strains, no change in the average misorientation, θ, was found. In the strain interval 2-8 the misorientation data can be approximated by a linear function of cumulative strain, that is $\Delta\theta \propto 5^{o} \times \Sigma\varepsilon$. The average misorientation approaches an apparent saturation value at high strains over ~8 (Fig. 2b). The saturation value is around 34° (Fig. 2b). In contrast, the proportion of HABs tends to increase with strain achieving ~80 pct at ε~12; an almost fully recrystallized structure is evolved at this strain.

The Al-3%Cu alloy. The main feature of the deformed microstructures in the Al-3%Cu alloy is high inhomogeneity attributed to the formation of deformation bands outlined by HABs after the first passage through the die (Fig. 4a). These bands looks like highly elongated grains. The longitudinal dimension of these bands is over 400 μm; the apparent width of these bands varies from 4 to 40 μm. Extensive formation of transverse LABs with misorientations ranging from 5 to 10° occurs within these bands. Serration of longitudinal HABs of these band-like features takes place.

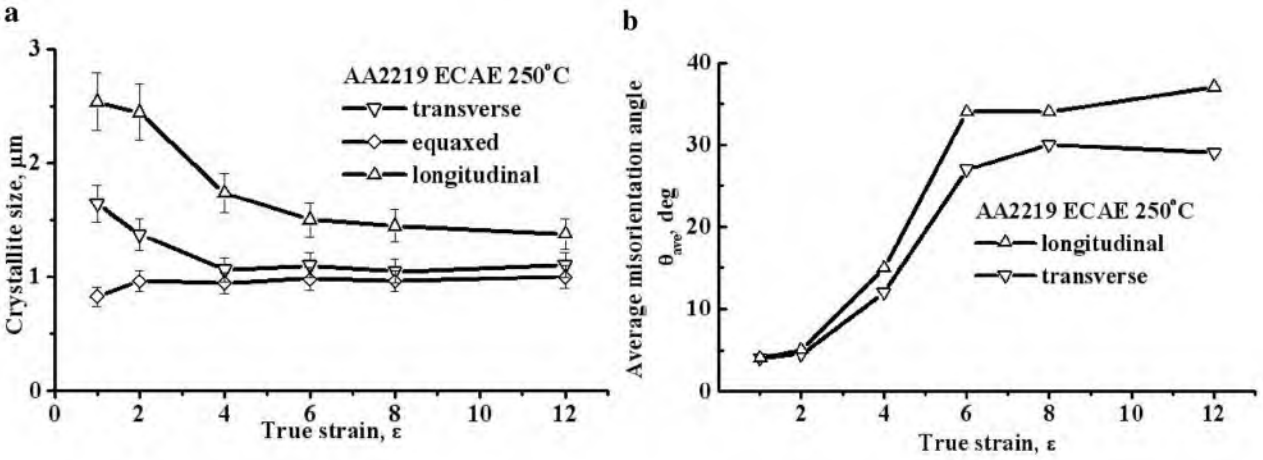

Fig. 2. Crystallite sizes (a) and average misorientation angle θ_{ave} of deformation induced boundaries (b) as a function of strain for AA2219.

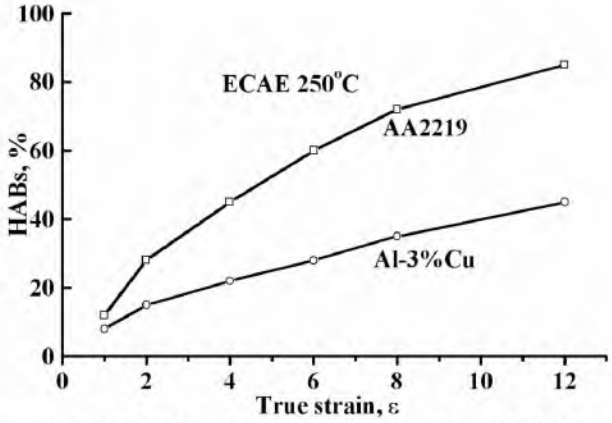

Fig. 3. Effect of strain on fraction of high angle boundaries (HABs)

It was found that a process of impingement of opposite boundaries results in the subdivision of these bands into highly elongated separate grains having a similar orientation. At ε~1, a poorly-defined subgrain structure is evolved within interiors of initial grains. Misorientation of LABs is about 1°, the formation of three-dimensional arrays of LABs was rarely observed. Only separate subgrain boundaries could be found within original grains being favorably oriented for multiple slip of lattice dislocations on the {111} <110> system. Simultaneously, there are two distinct areas in which well-defined arrays of deformation-induced boundaries could be found (Fig. 4a). The first areas are located between expanded medium to high angle boundaries or between the latter and an old boundary. The expanded separate boundaries with misorientation of ~12° usually lie on the primary slip planes in the shear direction (Fig. 4a). Notably isolated segments having increased misorientation or even high-angle origin were found along these continuous moderate-angle boundaries (Fig. 4a). If these medium to high-angle boundaries locate near initial HABs, so the mixed arrays consisting of LABs and HABs are observed between these extended boundaries (Figs. 4a, b). Notably, the old boundaries are highly serrated in these areas (Fig. 4b). Fig. 4a displays the existence of the second type of area within interior of an initial grain, where the intersection of two families of these moderate-angle boundaries is observed. The three-dimensional array of deformation-induced boundaries with misorientations ranging from low to high-angle is evolved in this area. True recrystallized grains outlined by HABs from all sides could be detected within these two different areas. Thus, first recrystallized grains of two different types are evolved in the Al-3%Cu alloy after ε~1.

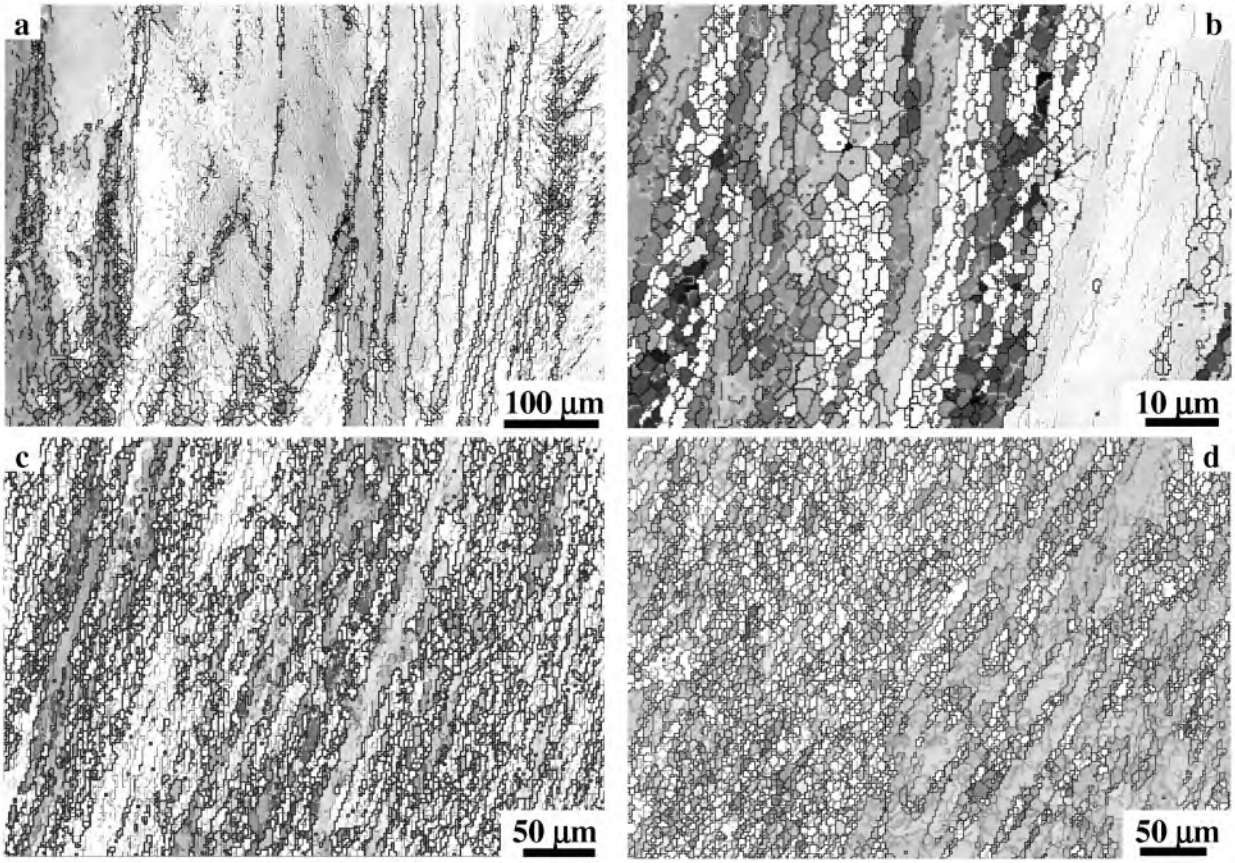

Fig. 4. EBSD maps of Al-3%Cu deformed at 250°C by ECAE to (a) ε=1, (b) ε=2, (c) ε=8, (d) ε=12. Light gray and black lines correspond to boundaries with misorientation ranging from 5 to 15° and with misorientation over 15°, respectively.

After ε~2, a well-defined subgrain structure is formed within the initial grains (Fig. 4b). LABs with misorientation less than 5° dominate, whereas separate fine grains could be observed (Fig. 4b). Mixed arrays consisting of LABs and HABs are evolved between two longitudinal HABs. Average width of such bands of newly evolved crystallites ranges from 16 to 20 μm (Fig. 5a). The last boundaries can be strongly serrated or essentially straight (Fig. 4b). Notably, the average misorientation of LABs within these arrays is over 5° (Figs. 4b and 5b); deformation-induced boundaries with average misorientation of ~12° and HABs are predominant. In general, the proportion of HABs increases with increasing strain from ~1 to ~2, despite the fact that the proportion of LABs with misorientation less than 5° remains essentially unchanged (Fig. 3). A feature of the Al-3%Cu alloy is a high fraction of moderate boundaries with misorientation ranging from 10 to 15°.

After further strain the microstructure is divided into recrystallized areas where moderate-angle boundaries and HABs dominate and unrecrystallized areas characterized by arrays of deformation-induced boundaries consisting of LABs with misorientations less than 5°. After ε~8, bands of recrystallized grains alternate with bands of unrecrystallized structure consisting of recovered subgrains with misorientation of LABs less than 5° (Fig. 4c). Two types of recrystallized grains are observed. New grains having essentially equiaxed shap dominate (Figs. 4c and 5a) and the orientations of neighbor grains in such recrystallized zones are distinctly different. The second type is made up of highly elongated grains comprising chains with similar orientation. The fraction of these grains is low.

Further strain up to ε~12 leads to an increased fraction of recrystallized grains (Fig. 4d) outlined by HABs from all sides and an increased proportion of HABs (Fig. 3). At ε~12, the distribution of HAB misorientation becomes more uniform. The significant proportion of LABs with misorientations less than 5^{o} is attributed to subgrain structure within the unrecrystallized grains. Medium to high-angle boundaries are mostly located within recrystallized grains (Fig. 4d).

The effect of ECAE on structural parameters of deformation-induced crystallites having essentially equiaxed shape is summarized in Fig. 5, which shows the variation in the (sub)grain size and the average misorientation, θ, between (sub)grains with strain. The effect of strain on the HAB population is shown in Fig. 3. The evolution of crystallite width resulting from HAB impingement is represented by a separate line (Fig. 5a). It is seen that the size of (sub)grains slightly decreases with increasing strain (Fig. 5a). This size and width of highly elongated grains are essentially the same due to subdivision of elongated (sub)grains aligned in the shear direction by transverse LABs which continuously convert into HABs with strain (Figs. 4-5).

The data in Fig. 5b clearly demonstrate that the average misorientation tends to increase at a moderate rate in the whole strain interval. The misorientation data can be approximated by a linear function of cumulative strain; $\Delta\theta \propto 2.2^{o} \times \Sigma\varepsilon$. Clearly this rate is less by a factor of about 2 than that for the AA2219 alloy. No well-defined saturation value of average misorientation was achieved in the Al-3%Cu alloy as in the AA2219 alloys containing nanoscale dispersoids. The proportion of deformation-induced HABs in the Al-3%Cu alloy also increases with strain (Fig. 3). However, the rate of this increment is not too high; the fraction of HABs in the Al-3%Cu alloy remains less than 50 pct even at ε~12. A partially recrystallized structure is evolved at high strain in this alloy.

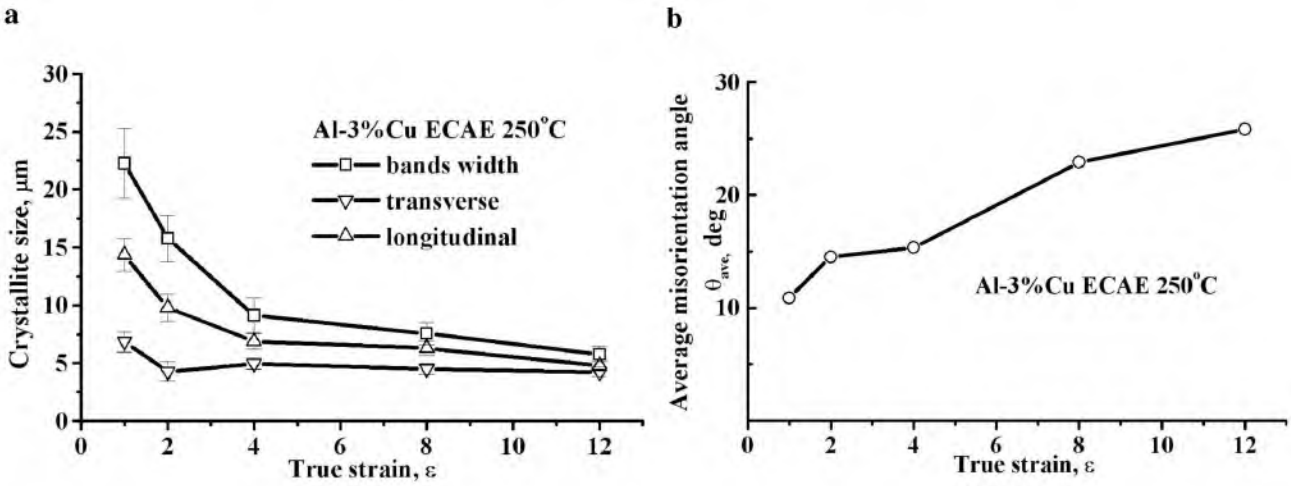

Fig. 5. Changes in crystallite sizes (a) and average misorientation angle θ_{ave} of deformation induced boundaries (b) with strain for Al-3%Cu.

Discussion

The AA2219 alloy. The experimental results clearly demonstrate that the main mechanism resulting in the formation of ultra-fine grain structure in the both materials is CDRX. However, the phase composition of Al-Cu alloys strongly effects the process of grain refinement. In the AA2219 alloy the Al_3Zr nanoscale dispersoids serve as an effective subboundary pinning agent stabilizing the evolved arrays of LABs [20]. As a result, deformation-induced LABs exhibit low mobility; no remarkable collision of subboundaries consisting of dislocations with opposite Burgers vector and their mutual annihilation occurs [21,22]. Three-dimensional arrays of immobile subgrain boundaries are evolved within interiors of old grains after ε~1 (Fig. 6a). The increased misorientation of

isolated segments of deformation-induced LABs compared with neighboring segments of extended LABs suggests that the main mechanism, which provides increasing misorientations of the LABs with strain, is the local trapping of mobile lattice dislocations (Fig. 6b). Lattice dislocations move across subgrains. The accumulation of mobile lattice dislocations into immobile LABs provides a gradual increase in their misorientation resulting in a gradual transformation of LABs into true HABs. The Al_3Zr dispersoids inhibit the HAB mobility by Zener pinning [20], and prevent grain growth. Thus, these nano-scale dispersoids play a role of pinning agent for all types of deformation-induced boundaries in the AA2219 alloy maintaining a stable submicron-scale size of newly evolved (sub)grains (Fig. 2a).

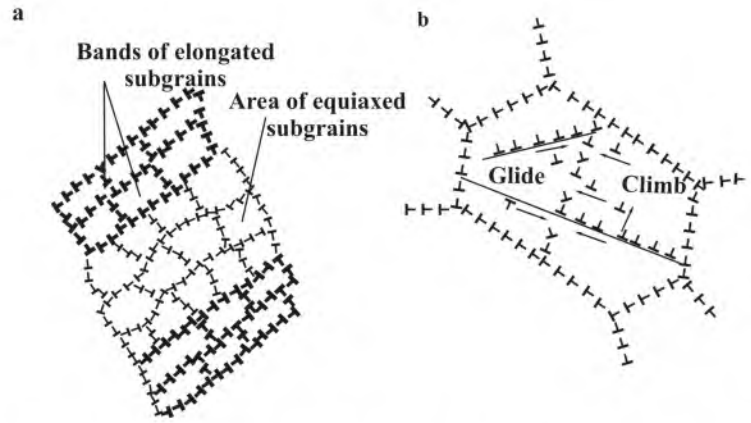

Fig. 6. Schematic representation of structure evolution in the AA2219 during deformation: (a) bands of elongated subgrains alternate with arrays of equiaxed subgrains; (b) introduction of mobile lattice dislocations into a low angle boundary.

The Al-3%Cu alloy. In the dilute Al-3%Cu alloy there are no pinning agents to suppress the migration of LABs. Deformation-induced LABs have high mobility leading to their collision and mutual annihilation [21,22]. This is why the above processes of CDRX are difficult within the initial grains of the Al-3%Cu alloy. A negligible number of recrystallized grains could result from this type of CDRX. Therefore, such type of CRDX [15], which can be termed as homogeneous CDRX, plays an unimportant role in the grain refinement process of the Al-3%Cu alloy. CDRX occurs in the dilute aluminum alloy in a highly heterogeneous manner and is associated with the formation of deformation bands after the first passage. The exact mechanism of the formation of the extended deformation bands outlined by HABs remains to be elucidated. Extensive serration of the HABs of these fibrous grains with thickness less than 6 μm leads to the occurrence of classical geometric recrystallization (GRX) (Fig. 7a) [23]; adjacent serrated grain boundaries eventually pinch off resulting in highly elongated grains. However, this is a rare case; classical GRX gives a minor contribution to the recrystallization process in the Al-3%Cu alloy.

The main contribution to recrystallization is provided by a specific GRX process, which can be considered as a type of CDRX. The conditions for evolving arrays of LABs are provided by extended HABs and immobile medium to high angle boundaries, which clamp mobile LABs maintaining a stable subgrain structure (Fig. 7b). Serrated HABs, which outline the deformation bands, trap the edge of evolving mobile LABs (Fig. 7b). Actually, this process is similar to the trapping of a lattice dislocation by a HAB [24]. The movement of a trapped dislocation along the serrated grain boundary surface is controlled by climb. As a result, this dislocation becomes essentially immobile; the adjacent transverse LABs can glide at high rates only after splitting with the dislocations trapped by HAB. However, next, a dislocation composing this LAB and being

nearest-neighbor to the adjacent HAB will be also trapped by the last serration. Thus, the LABs formed in the vicinity of serrated HABs loose their mobility.

In addition, the mobility of LABs evolved within old grains could be also hindered by continuous medium to high-angle boundaries aligned in the shear direction. The following model describing the formation of the long medium to high angle boundaries lying on the primary slip planes in the shear direction is suggested. A dislocation source S in Fig. 7c emits screw dislocations, which form a dense dislocation pile-up in the plane belonging to the {111} family along the shear direction [21]. This pile-up plays the role of barrier for glissile screw dislocation on the other {111} planes. These dislocations are trapped by this pile-up which converts into twist LAB consisting of two or three families of screw dislocations belonging to the {111} family [24]. A dislocation reaction within this dislocation network can result in the splitting of quadruple junction of two screw dislocations on an edge dislocation making this LAB immobile [24]. The operation of the primary dislocation source provides a high rate of misorientation development of this LAB with strain. As a result, boundaries with misorientations over 10^{o} located in the shear direction were found even after ε~1. These medium to high boundaries have non-compensated long-range stress fields which interact with short-range stress fields originated from transverse deformation-induced LABs restricting their mobility [21]. Thus, in the Al-3%Cu the formation of deformation bands followed by extensive serration of HABs and the formation of extended medium to high-angle boundaries parallel to these bands provide an ultimate condition for the evolution of stabilized three-dimensional arrays of LABs, in which no remarkable collision and mutual annihilation of LABs takes place. The subsequent transformation of LABs composing these arrays into HABs occurs by the intrusion of glissile lattice dislocation into immobile subboundaries (Fig. 6b) [21,25]. This process provides increasing misorientation of LABs with strain. A gradual conversion of LABs into HABs results in the formation of partially recrystallized structure. Increasing volume fractions of recrystallized grains with strain occurs due to increasing width of the band-like features containing three-dimensional arrays of deformation-induced boundaries. Thus, in dilute aluminum alloys and aluminum alloys containing coarse second-phase particles [2,4,8] the process of extension and compression of initial grain boundaries with strain initiates CDRX.

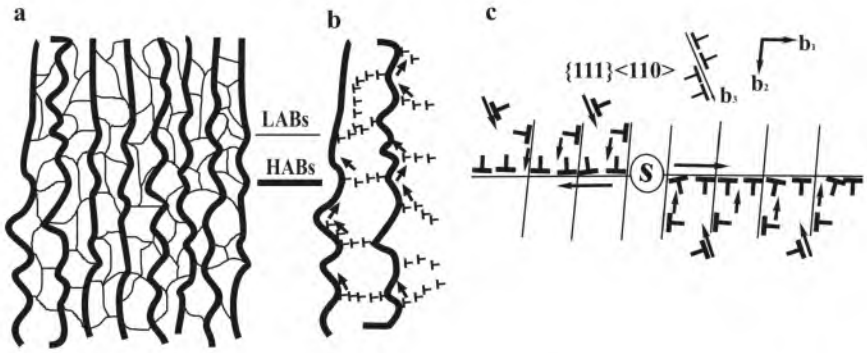

Fig. 7 Schematic representation of microstructure evolution in the Al-3%Cu: (a)-(b) schematic drawing of GRX process from ref.[23]. The arrows indicate the dislocation motions along the serrated grain boundary surface; (c) the formation of medium-to-high angle boundary. The arrows indicate dislocation glide.

Summary

It has been shown that the main mechanism resulting in grain refinement in Al-Cu alloys under intense plastic straining is continuous dynamic recrystallization (CDRX). The prerequisite condition for occurrence of CDRX is maintaining stable arrays of subboundaries at early stages of plastic deformation. In the AA2219 the Al_3Zr dispersoids play a role of effective pinning agents. As a result, CDRX occurs homogeneously. In the dilute Al-3%Cu alloy the arrays of low-angle boundaries are stabilized by boundaries of deformation bands, which have high-angle origin, and extended medium to high-angle boundaries. New grains in the dilute alloy results from a strain-induced continuous reaction occurring heterogeneously.

References

[1] N. Tsuji N, S. Okuno, T.Matsuura *et al.*: Mater. Sci. Forum Vol. 426-4 (2003), p. 2667.
[2] F.J. Humphreys, P. B. Prangnell, J. R. Bowen, A. Gholinia, C. Harris: Phil.Trans. R. Soc. Lond., v. 357A (1999), p.1663.
[3] R.Z. Valiev, R.K.Islamgaliev, I.V.Alexandrov: Progr.Mater.Sci., v.45 (2000) p.103.
[4] A. Golinia, P. B. Prangnell, M. V. Markushev: Acta Mater., v.48 (2000), p.1115.
[5] Y. Iwahashi, Z. Horita, M. Nemoto, T. G. Langdon: Acta Mater., v.46 (1998) p.3317.
[6] Y. Iwahashi, Z. Horita, M. Nemoto, T. G. Langdon: Acta Mater., v.45 (1997) p.4733.
[7] K. Nakashima, Z. Horita, M. Nemoto, T. G. Langdon: Acta Mater., v.46 (1998) p.1589.
[8] P.J.Apps, J.R.Bowen, P.B.Prangnell: Acta Mater., v.51 (2003) p. 2811.
[9] W.Q.Cao, A.Godfrey, Q.Liu: Mater.Sci.Eng., v.361 (2003) p.9.
[10] S.D.Terhune, D.L. Swisher, K.Oh-ishi, Z.Horita, T.G.Langdon, T.R.McNelley: Metall.Mater.Trans., v.33A (2002) p.2173.
[11] S.Ferrase, V.Segal, K.Hartwig, R.Goforth: Metall.Mater.Trans., v. 28A (1997) p. 1047.
[12] A.Belyakov, T.Sakai, H. Miura, K.Tsuzaki: Phil Mag, v.81 (2001) p.2629.
[13] A.Belyakov, T.Sakai, H.Miura: Mater.Trans.JIM, v.41 (2000) p.476.
[14] S.Gourdet, F.Montheillet: Mater.Sci.Eng., v.A283 (2000) p.274.
[15] S.Courdet, F.Nontheillet: Acta Mater., v.51 (2003) p.2685.
[16] I. A. Mazurina, O. Sh. Sitdikov, and R. O. Kaybyshev: Phys.Metal.Metall., v.94 (2002) p.413.
[17] O.Sh.Sitdikov, R.O.Kaybyshev, I.M.Safarov, I.A.Mazurina: Phys.Metal.Metall., v.92 (2001) p.270.
[18] R. Kaibyshev, K. Saytaeva, F. Musin and Y. *Motohashi: Hot Deformation of Aluminum Alloys III*, TMS, USA, 2003, p. 365.
[19] G. Thomas, M. J. Goringe: *Transmission Electron Microscopy of materials,* Wiley, New York, 1983, pp. 99-119.
[20] J. Humphreys, M. Hatherly: *Recrystallization and Related Annealing Phenomena*; Oxford, UK, Pergamon Press, 1996, pp. 493.
[21] O. Sitdikov, R. Kaibyshev: Mater.Sci.Eng., v.328 (2002) p.147.
[22] M. Biberger, W. Blum: Phil.Mag.A., v.65 (1992) p.757.
[23] A. Gholinia, F.J.Humphreys, P.B.Prangnell: Acta Mater. V.50 (2002) p.4461.
[24] M.A Shtremel': *The strength of Alloys, Part 1, Lattice Defects;* Moscow, Russia, MISIS, 1999, p.231.
[25] T.G. Nieh, L.M.Hsiung, J.Wadsworth, R. Kaibyshev: Acta Mater., v.46 (1998) p.2789.